Acta Geotechnica
https://doi.org/10.1007/s11440-019-00836-4

RESEARCH PAPER

Numerical values of shape factors for field permeability tests in unconfined aquifers

Lu Zhang[1] · Robert P. Chapuis[1] · Vahid Marefat[1]

Received: 26 June 2018 / Accepted: 3 June 2019

Abstract

Field permeability tests are used to evaluate the local hydraulic conductivity. Their interpretation requires knowing the value of a shape factor, c. Regular values for shape factors were obtained for fully saturated conditions in an infinite material. However, many tests are performed in unconfined aquifers, with a bottom impervious boundary, and partly unsaturated seepage. This paper questions the applicability of the regular c values to field conditions. It presents numerical ways to model field permeability tests in unconfined aquifers and deduce the c value, under steady and transient states, with partly unsaturated seepage. Two series of monitoring wells were analyzed and compared; they have either a filter pack or not. The influences of four variables (radial distance of the external boundary, dimensions and positions of the water injection zone, and aquifer material type) on the numerical c values were studied. The results show that the boundary radial distance markedly affects the numerical c value. Therefore, practical approaches were proposed by reconciling the numerical and realistic test conditions, to determine the representative boundary radial distances for each type of test model. Additionally, the numerical values are compared with the theoretical values of Bouwer and Rice (Water Resour Res 12(3):423–428, 1976) and Hvorslev (Time-lag and soil permeability in ground water observations, U.S. Army Eng Waterw Exp Stn, Vicksburg, 1951).

Keywords Constant-head · Field permeability test · Numerical modeling · Shape factors · Variable-head

1 Introduction

The shape factor, c, is a factor related to the shape and dimension [37], the position [5, 6] of the well point or the water injection zone, and the boundary conditions. It serves as a critical parameter in the calculation of hydraulic conductivity K for aquifers, which is interpreted from field permeability test data. Researchers proposed different theoretical, electrical analog, and numerical methods to deduce the shape factor in unconsolidated materials [1, 7–9, 11, 39, 40, 43, 47, 48, 51–59, 61]. Two famous equations for the shape factor were provided by Hvorslev [37] and Bouwer and Rice [6]. The latter, however, yields a higher c value due to its unrealistic assumptions [16]. Theoretical values for shape factors were obtained for fully saturated conditions in an infinite material. However, many tests are performed in unconfined aquifers, with a bottom impervious boundary, and partly unsaturated seepage. Thus, the paper examines if the commonly used theoretical c values are still applicable to these field conditions.

The code Seep/W [35] enables us to quantify the shape factor numerically. Unlike other numerical codes on groundwater seepage, it allows the capillary retention curves $\theta(u)$ and unsaturated hydraulic conductivity functions $K(u)$ to be independent, which models the monitoring well adequately [15]. Its reliability was examined for various cases, from one to three dimensions [27]. A variety of problems, such as seepage through dikes [22], the vadose zone effect on the leakage rates in landfill barriers [10], and the seepage characteristics of the buttressed embankment using a centrifuge test model [38], were solved via the code. Integrated with other codes, it was also applied to study hydraulic short circuits, groundwater contamination, and slope collapse by seepage erosion [2, 31, 33].

✉ Robert P. Chapuis
robert.chapuis@polymtl.ca

[1] Department of Civil, Geological and Mining Engineering, École Polytechnique, P.O. Box 6079, Station CV, Montreal, QC H3C 3A7, Canada

The numerical simulation for the variable-head (VH) test by the code was initially presented by Chapuis [12]. The negligible role of storativity for the simulated VH tests [24], the pipe storage capacity effect, and tidal influence on pumping test results were discussed for the confined aquifer [23, 25]. For unconfined aquifers, the double-line effect while dewatering down to the screen in the VH test, and the unusual drawdown curves of the pumping test were also analyzed numerically [14, 26]. The numerical value of shape factor was determined for the steady-state conditions of the constant-head (CH) test in either confined or unconfined aquifers [14, 24, 28]. For aquifer models with given geometries, the smaller numerical c values compared to the Hvorslev's c value were due to a reduced flow rate caused by the model finite size [14, 24].

However, several problems still wait to be solved. Firstly, if no information is available about the influence radius of the well, increasing the boundary radial distance will significantly increase the computation time because unsaturated seepage calculation (highly nonlinear equations) takes a very long time. However, in field conditions, the pumping rate for a CH test will be small and one may suspect that the influence radius will be small, but how much? Thus, we need to specify an appropriate boundary radial distance for the numerical test model. Secondly, the shape factor values in the literature were obtained for steady-state conditions only, thus for a CH test, not a VH test. In practice, CH and VH tests are performed. Unfortunately, in the calculation of shape factors, a biased electrical analogy was used [16], and no attention was paid to transient conditions preceding steady state in the CH test. Furthermore, the shape factor values deduced from numerically simulated VH tests have never been presented and compared with those used for the CH tests. In addition, we are curious about how many parameters would affect the numerical results of the two types of tests.

To provide practical answers, two series of axisymmetric unconfined aquifer models equipped with monitoring wells (MWs) were studied because unconfined aquifers have a high potential for being contaminated, and MWs in unconfined aquifers are frequently tested using CH or VH tests. The MW pipe of the first series of models had a screen but no filter pack. In the second series, the pipe screen was surrounded by a filter pack. Field permeability tests of two types (CH and VH) were conducted numerically in the MWs, and the numerical c values were calculated. The CH test reached steady state after a transient condition, which lasted a long time depending upon the radius of influence and the unsaturated hydraulic properties of the tested soil. The VH test was totally in transient condition.

Each series of models investigated four variables: 11 distances of the boundary (R), four lengths (L) for the injection zone, three positions of the water injection zone, and 15 types of soils, thus 15 sets of water retention curves (WRC) and saturated hydraulic conductivities (K_{sat}) for the unconfined aquifer. Three parameters were kept constant when one parameter was varied. The unconfined aquifer was homogeneous and isotropic, and its unsaturated parts were fully defined with the use of capillary retention and unsaturated hydraulic functions, $\theta(u)$ and $K(u)$.

The influences of the four variable parameters on numerical c values are analyzed. The c differences derived from CH and VH tests of each series are discussed. The result of the transient analysis of the CH test is compared with that of its steady-state analysis. The numerical c values are also compared with the theoretical values by Hvorslev's [37] and Bouwer and Rice's [6] equations.

2 Field permeability tests modelization

2.1 Unconfined aquifer models

They are 2D axisymmetric (r, z) models, the z-axis being the central vertical axis of the monitoring well, which saves computation time compared to 3D models. The MW is installed in the unconfined aquifer located between elevations 0 and 4 m. Before the tests, the water table was 1 m below ground level, at elevation 3 m. The MW is a schedule 40 2-inch pipe, which has internal and external diameters of 5.2 and 6.0 cm, respectively, and a wall thickness of 0.4 cm. The riser pipe extends up to $z = 4.2$ m and has a 1-m-long screen located at the bottom, without a filter pack (the first series).

The screen is surrounded by a filter pack of 15.24 cm (6-inch borehole) in external diameter in the second-series model. The filter pack extends from $z = 0$ to 1 m. The screen is 0.8 m long between $z = 0.1$ and 0.9 m. The annular space around the solid pipe above the filter pack is sealed using bentonite pellets.

The initial R for the two series of models is 3 m. In addition, other ten boundary radial distances, 2, 4, 5, 8, 10, 20, 40, 60, 80, and 100 m, were studied for models either with or without a filter pack to study the influence of R on the numerical c values.

For the first series that has a screen but no filter pack, the lengths of the partially penetrated screened portions are 1 m, 2 m, and 3 m, respectively. The pipe with a 4-m screen was also analyzed as a fully penetrating MW. The filter packs of the second series similarly range from 1 to 4 m in lengths, and the screens are 0.1 m shorter than the filter packs at both ends. Furthermore, the water injection zones of the two series were located at top (T), middle (M), and bottom (B) positions in the aquifer, which refer to a close, medium, and far distance from the water table position, respectively. The various lengths and positions of the water injection zone were termed 1 m-B, 1 m-M, 1 m-T, 2 m-B, 2 m-M, 2 m-T, 3 m-B, 3 m-T, and 4 m. For 2 m-T, 3 m-T, and 4 m, the screens straddle the water table. Figure 1 presents schematics of the dimensions and positions of the two series of water injection zones.

A global mesh size of 10 cm was used for the model. The mesh was refined to 1 cm close to the injection zone and in the unsaturated soil volume where the pore water pressure u is negative. The refined regions were mixed quad and triangle mesh, and the pipe was generated as rectangular meshes. The large element size was used where hydraulic head varied lightly. The element size of the deep saturated zone and the faraway saturated zone was increased up to 30 cm when R exceeded 20 m, which reduced the computation time. The mesh was selected after a h-convergence study, which differs from the code internal convergence rules, in order to reach a solution that does not depend on the element size. The time steps were also

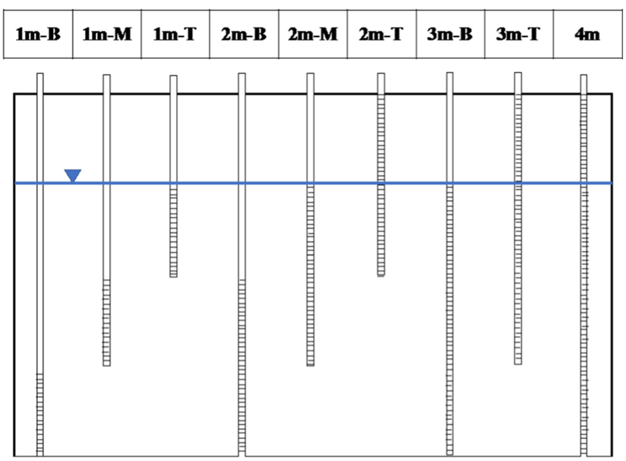

(a) Screen only

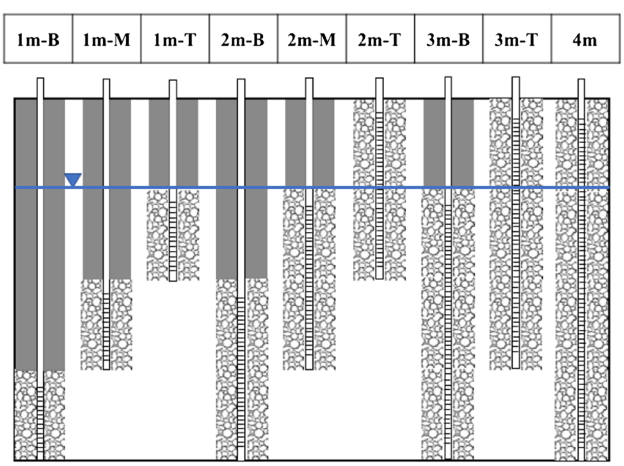

(b) With a filter pack

Fig. 1 Different lengths and positions of two series of water injection zones

selected after a convergence study to reach a time-step independent solution. The lengthy but crucial convergence studies were explained in [17–19, 21] and are not presented here.

2.2 $K(u)$ and $\theta(u)$ functions

In the unconfined aquifer model, the pipe, filter pack, and granular soil are homogeneous and isotropic, and the unsaturated behaviors were taken into account. The pipe inside is very permeable with a saturated K_{pipe} of 100 m/s, which was considered as a "reservoir" element and has two independent $K(u)$ and $\theta(u)$ functions [15]. The $\theta(u)$ declines from θ_s = 0.9 to θ_r = 0.15 as the pore water pressure u drops from 0 to − 1 kPa. It means that the internal section of the MW, which stores water, represents 75% (0.90–0.15) of the external cross-sectional area of the pipe. The drop of u from 0 to − 1 kPa could provide a rapid convergence [15].

The aquifer material No. 0 has a porosity n of 0.38 (void ratio e of 0.613) and effective size d_{10} of 0.145 mm. Its saturated hydraulic conductivity is obtained from the predictive equation $K_{\text{sat}}\,(\text{cm/s}) = 2.4622\left(\frac{d_{10}^2 e^3}{1+e}\right)^{0.7825}$ [13], which is 2.61 × 10^{-4} m/s. The filter material has a saturated K value of 1.74 × 10^{-2} m/s and is much more pervious than the aquifer material. The materials have constant K values in saturated zones where the pore water pressure is positive.

Besides No. 0 sand, the properties-K_{sat} and $\theta(u)$-of the other 14 types of soils, ranging from coarse sand to silt, were collected from previous research [36, 46, 49, 50] to study their impact on numerical shape factors. The soils have different grain size distributions and K_{sat} values between 1.45 × 10^{-7} and 2.31 x 10^{-4} m/s (Table 1), which were named from Nos. 1 to 14.

The water retention curve (WRC) is a critical material function that defines the unsaturated soil behavior. The air entry value (AEV), residual suction u_r (kPa), and residual volumetric water content θ_r were predicted by the best-fit equations [29] based on known d_{10} (mm) and e. The WRCs of coarse soils were then obtained by substituting the derived parameters into the LN fit [41]. The method is valid when the product of e and d_{10} is larger than 0.0005.

For finer soils of Nos. 5, 6, 7, 8, and 10 which have ed_{10} < 0.0005, their θ (u) functions were estimated by the modified Kovacs (MK) method [3]. The MK model redefined some key parameters that had not been well defined in the original Kovacs [42] model. The modifications focus on the statistical function used to describe the pore-size distribution of the media in the capillary component, and the constitutive parameters based on the basic soil properties [3]. The suction unit is cm water and must be

Table 1 Basic soil geotechnical and hydraulic parameters

No.	Granular materials	K_{sat} (m/s)	n –	d_{10} (cm)	C_u –	e –	ed_{10} –
0	Sand for initial model	2.61×10^{-4}	0.380	0.1450	–	0.613	0.0889
1	Code 1460 Berlin coarse sand	2.91×10^{-5}	0.297	0.0224	–	0.422	0.0095
2	Code 1461 Berlin coarse sand	2.31×10^{-4}	0.373	0.0224	–	0.595	0.0133
3	Code 1462 Berlin medium sand	1.16×10^{-4}	0.430	0.0144	–	0.754	0.0108
4	Code 1463 Berlin medium sand	8.01×10^{-5}	0.399	0.0144	–	0.664	0.0095
5	Code 1465 Berlin fine sand	4.63×10^{-6}	0.384	0.0028	4.5	0.623	0.0017
6	Code 1466 Berlin fine sand	2.48×10^{-5}	0.414	0.0062	1.8	0.706	0.0044
7	Code 1467 Berlin loamy sand	1.27×10^{-6}	0.312	0.0028	14.2	0.453	0.0012
8	Code 2221 Riverwash sand	1.45×10^{-4}	0.328	0.0054	8.7	0.488	0.0026
9	Code 4650 Plumhof sand	1.13×10^{-6}	0.380	0.0090	–	0.613	0.0055
10	No. 2002 Silt	1.45×10^{-7}	0.442	0.0002	122.0	0.792	0.0002
11	No. 4118 Sand	1.81×10^{-4}	0.342	0.0156	–	0.520	0.0081
12	No. 8 Sand Grenoble 1	2.87×10^{-5}	0.430	0.0143	–	0.754	0.0108
13	No. 9 Sand Grenoble 2	1.48×10^{-4}	0.408	0.0100	–	0.689	0.0069
14	No. 11 Sand Grenoble 4	6.33×10^{-5}	0.385	0.0210	–	0.626	0.0132

Code 1460 to 4650 sand [46], No. 8 to No. 11 sand [36], No. 2002 silt and No. 4118 sand [50]

converted to kPa (1 kPa = 10.197 cm water) for the code. The model can be applied to a large range of materials from coarse sand to fine-grained soils. Compared to the best-fit equation [29], however, it provides a slowly decreasing residual water content instead of a constant one, which is less realistic for coarse materials.

The $K(u)$ functions were estimated by the van Genuchten's closed-form equation [60] embedded with the code, based on known $\theta(u)$ functions. The corresponding $\theta(u)$ and $K(u)$ of each soil must give identical AEVs, as presented in Figs. 2 and 3.

2.3 Boundaries for field permeability tests

The CH test, for the steady-state analysis, had a far boundary with a hydraulic head of 3 m, and the head at the screen and in the riser pipe was h = 4 m, which represents the steady state of a CH injection test that has a head difference of 1 m. A constant flow rate Q in pipe and aquifer will be found by the numerical analysis. An alternative way of modeling the CH test was to keep the far boundary of h = 3 m and apply this constant injection Q in the MW to create a constant-head difference of 1 m.

The transient analysis of the CH test started with an initial equilibrium state, which is a steady-state analysis, by specifying h = 3 m everywhere. The next step was the transient analysis of an injection process with h (far boundary) = 3 m, and the boundary conditions for screen of either h = 4 m or Q = const. The test durations vary with different boundary radial distances and aquifer

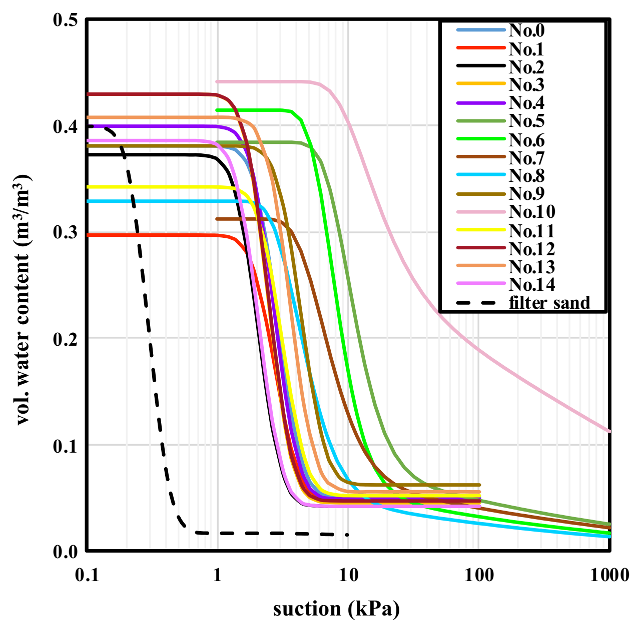

Fig. 2 $\theta(u)$ functions of the aquifer materials and filter sand

materials and thus should be determined by trial and error for each model. In the field, the CH test duration is usually around 20–30 min. However, a 5-h duration was identically used for all numerical CH tests, which is less practical but helps to compare the seepage in different models synchronously. In all cases, 100 time steps were applied to shorten the computation time greatly, which had been verified to yield same results as the calculation of 1000 time steps.

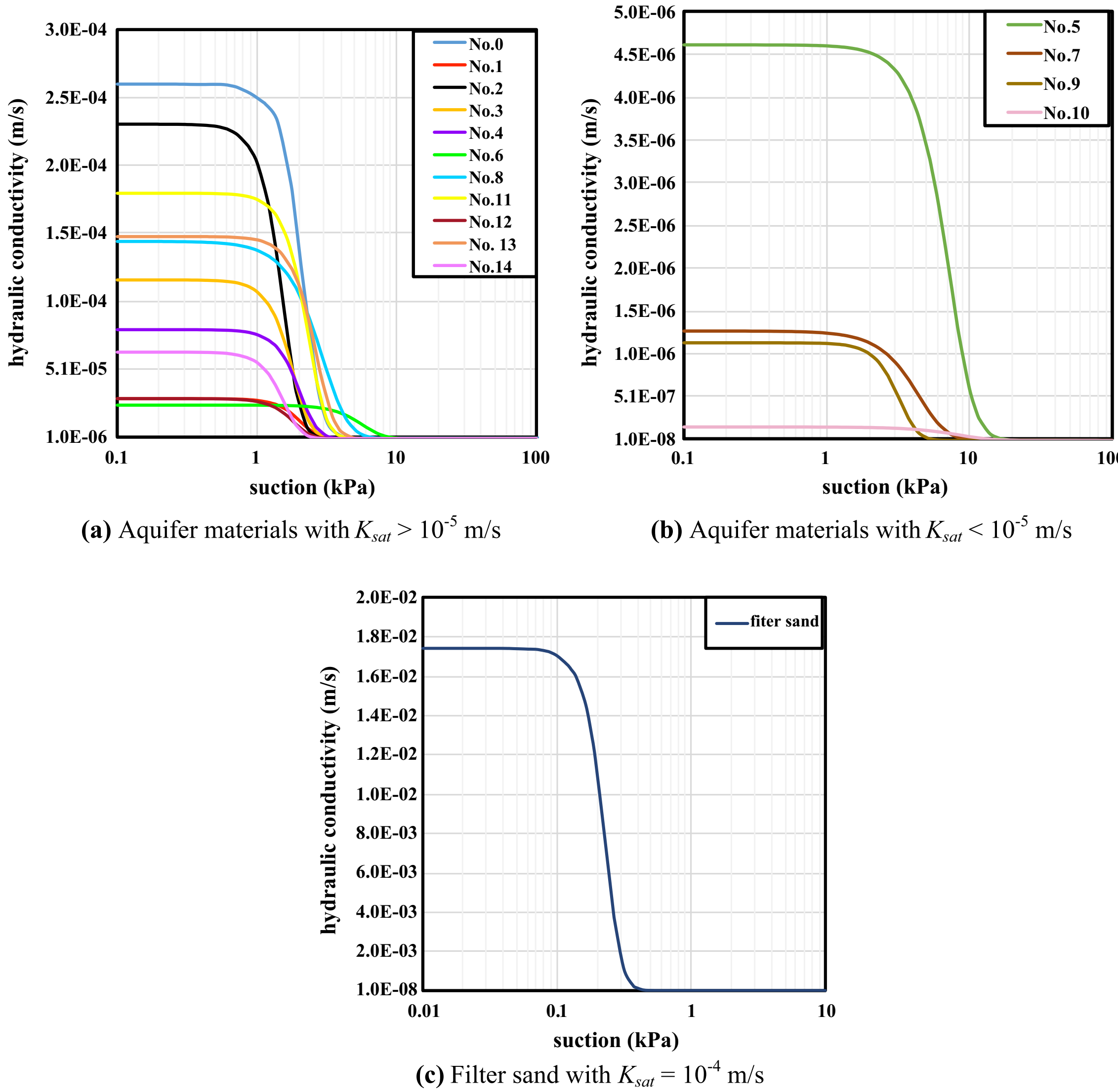

Fig. 3 Corresponding $K(u)$ functions of the aquifer materials and filter sand

The simulation of the VH test was in three steps. The initial equilibrium condition was assumed with known piezometric level 3 m in the entire model. The water level in the pipe was then raised by 1 m in 1 s, implemented by imposing a boundary function of the total head h versus time t on the screen, and h = 3 m on the far boundary. The final step kept h (far boundary) = 3 m and removed the boundary condition on screen, which started the falling-head test.

3 Shape factors equations

There are two ways to model a CH test numerically, applying either a constant flow rate Q or a constant hydraulic head difference H_c on the boundary of the well screen. The former yields an H_c value after reaching equilibrium, and the latter gives a stabilized Q-value after computation. With these known parameters, the numerical c values for a CH test can be calculated from Eq. 1, derived from the Lefranc's equation [44, 45]:

$$c = \frac{Q}{KH_c} \tag{1}$$

where K is the hydraulic conductivity; once one parameter of the Q and H_c is defined by users, the other parameter can be obtained directly from the numerical results.

For the transient analysis of VH tests, the variations of head difference H and time t are obtained from the numerical result, and the numerical c values are determined by Eq. 2, according to the Hvorslev's equation [37]:

$$c = \frac{\ln(H_1/H_2)}{(t_1 - t_2)} \cdot \frac{S_{\text{inj}}}{K} \tag{2}$$

where H_1 and H_2 are the hydraulic head differences at times t_1 and t_2, respectively, $[\ln(H_1/H_2)]/(t_1 - t_2)$ is the slope of the Hvorslev's semi-log graph, and S_{inj} is the internal cross-sectional area of MW pipe. For field tests, if the semi-log graph is not a straight line, the velocity graph method [12, 20, 30] or the *Z-t* method [32] is used to straighten the plot and extract the systematic error on water columns, which may be due to four or five sources of field errors. However, for numerical tests, there is no such systematic error.

The formulas for the theoretical shape factor were derived from the solutions of the Laplace equation, based on approximate shapes of the cylindrical injection zone, either a sphere of equal surface or an ellipsoid [14], in an infinite medium. The complete ellipsoid formula was given by Dachler [34]:

$$c = \frac{2\pi L}{\ln\left[\frac{L}{D} + \sqrt{1 + \left(\frac{L}{D}\right)^2}\right]} \tag{3}$$

where L and D is the length and diameter of the water injection zone, respectively. It was simplified by Hvorslev [37] as,

$$c = \frac{2\pi L}{\ln(2L/D)} \quad \text{if } L/D > 4 \tag{4}$$

The sphere formula is expressed as,

$$c = 2\pi D\sqrt{\frac{L}{D} + \frac{1}{4}} \quad \text{if } 1 \le L/D \le 8 \tag{5}$$

Bouwer and Rice [6] assumed that the Thiem equation could be used in the unconfined aquifer with partially penetrated well and then made an electrical analogy, which provided a shape factor:

$$c = \frac{2\pi L}{\ln(R_0/r_w)} \tag{6}$$

where R_0 is the radius of influence and $r_w = D/2$ is the external radius of the water injection zone. This equation is similar to Eq. 4. Two empirical formulas for $\ln(R_0/r_w)$ were obtained based on the electrical analogs in steady-state conditions:

$$\ln(R_0/r_w) = \left[\frac{1.1}{\ln(d/r_w)} + \frac{A + B\ln(b-d)/r_w}{L/r_w}\right]^{-1} \quad \text{when } b > d \tag{7}$$

$$\ln(R_0/r_w) = \left[\frac{1.1}{\ln(d/r_w)} + \frac{C}{L/r_w}\right]^{-1} \quad \text{when } b = d \tag{8}$$

where d is the distance from water level to the bottom of the water injection zone, which must be larger than the length of the water injection zone L, L ranges from near d to near 0, b is the saturated thickness of the unconfined aquifer, ranging from d to ∞, and A, B, and C are three dimensionless coefficients, functions of L/r_w defined by Bouwer and Rice [6].

4 Theoretical values of shape factors

The two known theoretical shape factors are not influenced by material properties. They assume the aquifer radial boundary to be sufficiently distant as to not affect borehole flow and thus are independent of the aquifer radial distances. The Hvorslev shape factor depends only upon the dimensions of the water injection zone. The Bouwer and Rice's equation, however, needs to additionally take into account the injection zone position. The shape factors of injection zones with lengths of 1, 2, 3, and 4 m were computed, considering their different positions. The diameter of injection zone for the MW without filter pack is equal to the external diameter of the screen, which was 6 cm. For the case that has a filter pack around the screen, the injection zone had a diameter of 15.24 m (6-inch borehole). The Hvorslev's and Bouwer and Rice's c values for the two series are presented in Table 2, where the Bouwer and Rice's c values of 1 m-B, 2 m-B, 3 m-B, and 4 m were calculated by Eq. 8 and the others by Eq. 7 due to the different positions of the injection zone.

It is observed (Table 2) that the Bouwer and Rice's c in the two series is always higher than the Hvorslev's c. This happens because in their electrical analog the authors confused the water table with a constant-head boundary, which yielded a higher flow rate compared to the realistic problem, thus producing a higher shape factor [16].

5 Influences of the four variables on numerical shape factors

5.1 Boundary radial distance influence on shape factor

5.1.1 First series: no filter pack

The numerical c values derived from the three types of numerical analyses are plotted together with the theoretical c values versus R in Fig. 4. The CH steady-state flow rates Q in pipe decreased steadily with the increase in the boundary radial distance R from 2 to 100 m due to the decline in radial gradients. Due to their proportional correlations, the derived c values steadily decrease in the lin-log plot, from 1.84 to 1.36 m (Fig. 4). The numerical c-curve intersects with the constant Hvorslev's c of 1.79 m at R = 2.6 m. The CH transient c is equal to the CH steady-

Table 2 Theoretical shape factors

Injection zone	Lengths (L) and positions	1 m-B	1 m-M	1 m-T	2 m-B	2 m-M	2 m-T	3 m-B	3 m-T	4 m
No filter pack	Hvorslev	1.79	1.79	1.79	2.99	2.99	2.99	4.09	4.09	5.14
D = 0.06 m	Bouwer and Rice	1.90	2.39	2.76	3.60	4.29	5.01	5.29	6.26	6.93
With a filter pack	Hvorslev	2.44	2.44	2.44	3.85	3.85	3.85	5.13	5.13	6.35
D = 0.1524 m	Bouwer and Rice	2.55	3.33	3.99	4.67	5.73	6.96	6.82	8.16	8.87

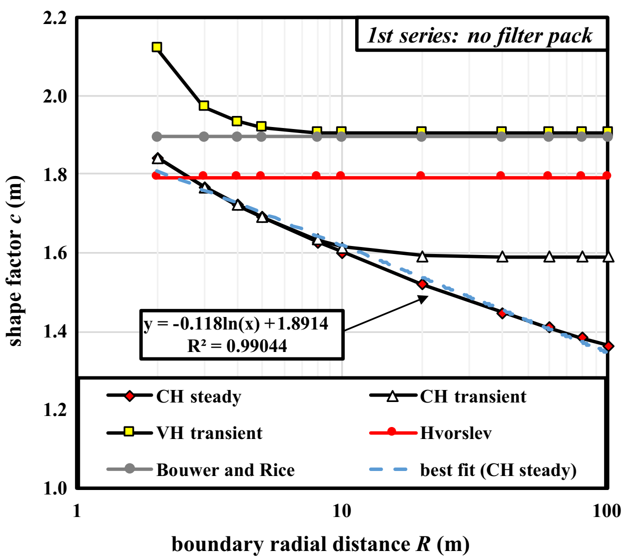

Fig. 4 Shape factors versus boundary radial distance (no filter pack)

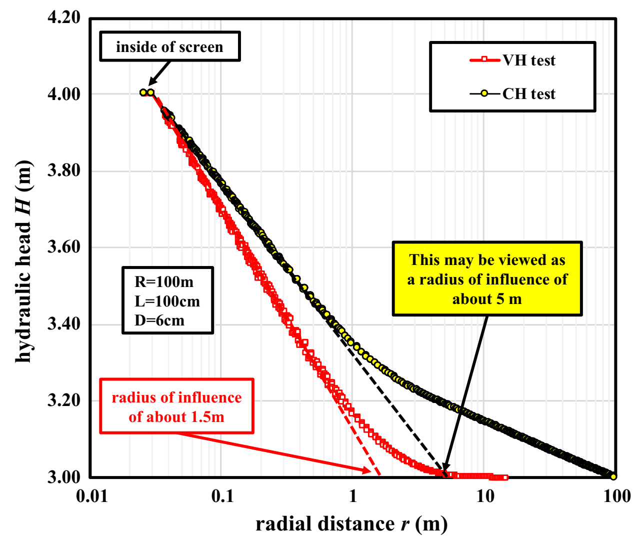

Fig. 5 Examples of variation of the hydraulic head versus distance

state c when R is no greater than 8 m. Beyond this range, the two types of shape factors become different and the former finalizes at a constant value of 1.59 m starting from R = 20 m. The Bouwer and Rice's c value is 1.90 m, greater than the CH and Hvorslev's c values.

For the VH test, R does not have the same influence on the shape factor because the VH test is quite rapid and modifies the hydraulic head within a small volume around the well. This can be justified by a simple numerical model with CH and VH tests. Figure 5 presents one of our first-series models, which has a screen of 1 m in length and 6 cm in diameter located at the bottom of the aquifer, where the boundary radial distance (R) is 100 m. It displays the hydraulic head variation along the radial distance of the model for both CH and VH tests, from which the respective influence radius was estimated. In Fig. 4, the numerical c for the VH test has a narrow range from 1.91 to 2.12 m. It starts at the highest value for a small R value and then drops to a constant value of 1.91 m from R = 8 to 100 m, very close to the Bouwer and Rice's c value.

In addition, the transient water table positions at r = 3 cm at various times were compared with the steady-state water table positions for models of different boundary radial distances (Fig. 6). The water tables under steady-state analysis of aquifer models yield a log-linear line with increased R. For the CH transient plots, the water tables are at z = 3 m at the beginning (t = 0 s) everywhere. They then rise along with the elapsed time up to 5 h in all cases

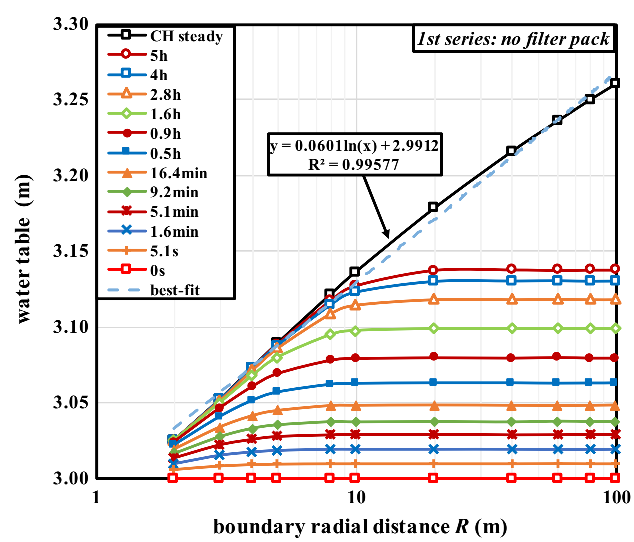

Fig. 6 CH steady-state and transient water tables at r = 0.03 m versus boundary radial distance

of boundary radial distances from 2 to 100 m. It is also observed that the transient water table of 5 h deviates from the steady-state water table when $R > 8$ m.

5.1.2 Second series: with a filter pack

The addition of a filter pack increases the diameter of the injection zone from 0.06 to 0.1524 m. Figure 7 presents all types of c values for the second series. The CH steady-state Q decreased from 6.43×10^{-4} to 4.38×10^{-4} m^3/s when R increases from 2 to 100 m. The c value consequently reduces from 2.46 to 1.68 m. Similar to the results of the first series, the CH steady-state and transient c values become different when $R > 8$ m, but the difference is that they equal the Hvorslev's c when $R = 2.1$ m instead of 2.6 m. The CH transient c value becomes an invariable of 2.03 m from $R = 20$ m. The VH test shape factor drops from 2.88 to 2.47 m for R values below 8 m and becomes constant at higher R values. The stabilized VH test c value is 3% lower than the Bouwer and Rice's $c = 2.55$ m and 1% higher than the Hvorslev's c value of 2.44 m.

The water tables of the two numerical analyses for the CH tests are plotted in Fig. 8. The plots of water tables at $r = 7.62$ cm (interface between the soil and the filter pack) versus R of the second-series models have similar relationship in comparison with the first series. The steady-state water table also appears as a straight line.

5.1.3 Discussion

Compared to the first-series models, all shape factors take greater values and the water tables during the test are higher for the second series due to the increased diameter of water injection zone, i.e., the addition of the filter pack.

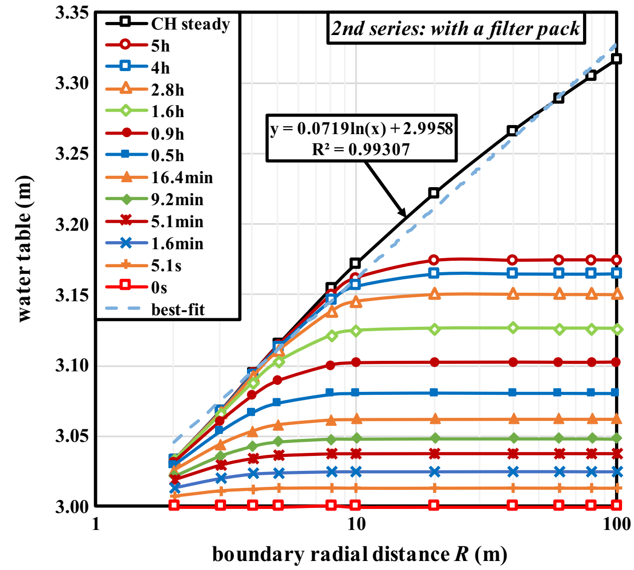

Fig. 8 CH steady-state and transient water table at $r = 0.0762$ m (interface between soil and filter pack) versus boundary radial distance R

Theoretically, the final results of the CH test in transient and steady-state analyses should be the same if the former reaches equilibrium, because the two test models are identical in geometry, material, and boundary condition except that the transient analysis is time dependent. In transient analysis, the flow rate is decreasing in the pipe and increasing in the aquifer with elapsed time. The two flow rates become equivalent when the steady state is reached.

In our case, the final results including the flow rate, water table, and contours are different for the two analyses when R exceeds 8 m. The reason is that the specified 5-h test duration is not long enough for numerical models of large boundary radial distances to reach equilibrium. Consequently, the Q (pipe) is larger than instead of equivalent to the Q (aquifer); hence, the derived CH test transient c values are greater than the CH test steady-state c. We subsequently ran each numerical model of the first series for a time long enough to have a Q (pipe) value varying by less than 1% (Fig. 9). The same curves with test times in log scale are also plotted to make those of smaller radial distances clearer to see. It should be noted that the curves seem to decrease faster after around 1000 s (Fig. 9b) but this is due to the time log scale, the real variation of Q with time being much slower than it seems to be in Fig. 9b.

The curves in Fig. 10 are the hydraulic head (H) variations with time when the CH tests were conducted with a constant flow rate. The tests were stopped when the

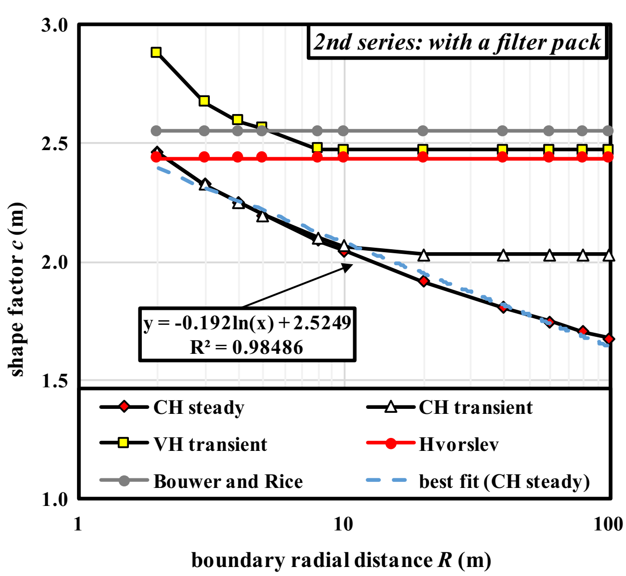

Fig. 7 Shape factors versus boundary radial distances (with a filter pack)

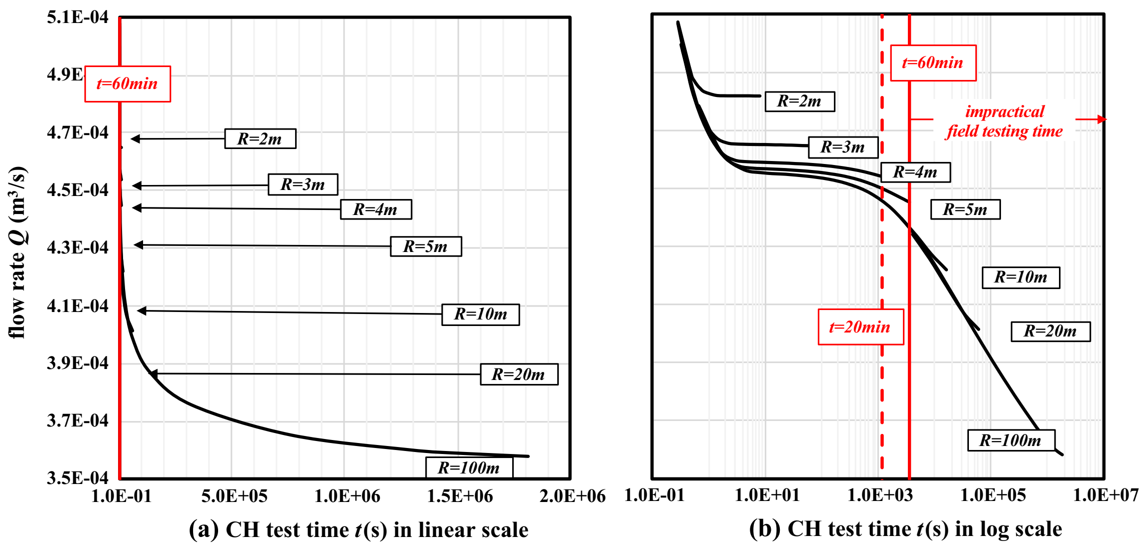

Fig. 9 Flow rate Q variations in pipe with CH test time t in linear and log scale

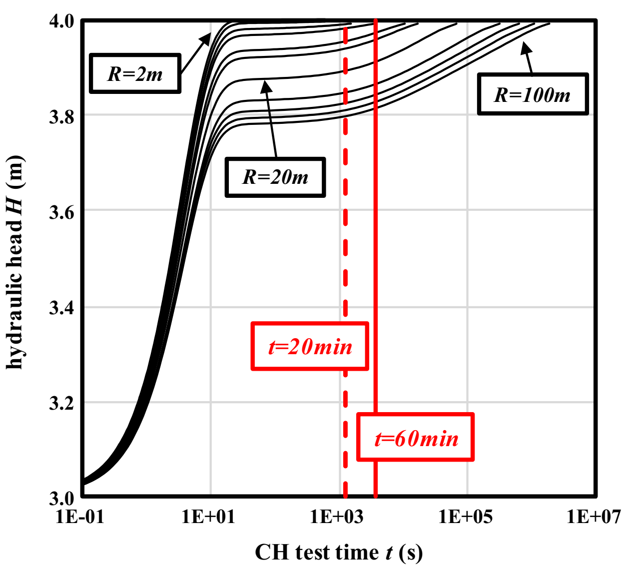

Fig. 10 Hydraulic head H variations in pipe with CH test time t

H (pipe) has a variation less than 1%. If we stop the tests after 2 min, for example, the post-test stabilized hydraulic heads differ from the theoretical equilibrium of 4 m by 0.01–5.4% (R = 2–100 m). The numerical shape factors are slightly different compared to the tests stopped after 20 min, because the specified boundary condition of constant Q (pipe) needs a few minutes to become constant. This is more representative of real field testing conditions. For any boundary radial distance, R, the hydraulic head seems to be stable between 2 and 20 min, usually the longest duration of field tests. Thus, stopping a field test after a few minutes seems justified, but the numerical analyses indicate that the time t and the R value still have some influence on the hydraulic head, which changes only a little as compared to the change in the first two minutes.

When the Q or H value reached 99% of the steady-state value, the tests were considered to reach equilibrium, and the corresponding times were defined as the test durations. Figure 11 shows the durations of CH tests that were simulated in two ways for different boundary radial distances (black plots). The first boundary condition has a constant H difference, and the second has a constant Q on the screen. The two ways provide approximately equivalent results, which follow a power function, except for R = 2 and 3 m. The reason is that when R is smaller than 4 m, the tests reach the set equilibriums faster than when the

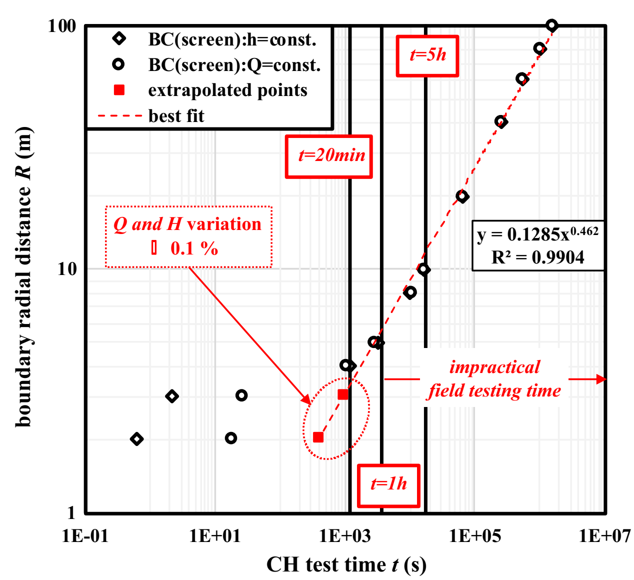

Fig. 11 CH test times by two simulating methods versus boundary radial distances

boundary radial distance is larger. When H reaches 3.99 m, it varies from the head difference of 1 m by 1%. Figure 10 shows that it is difficult to obtain accurate test duration for R = 2 and 3 m because the H plot is nearly horizontal when H variation $<$ 1%. If we extrapolate the plot, the two test durations at R = 2 and 3 m (the two red points) represent the time to reach the equilibrium where Q and H values reached 99.5% of the steady-state values.

It is observed from Figs. 9, 10, and 11 that the test duration, for R values exceeding 5 m, exceeds 1 h, which is impractical for field tests. Normally, the CH test takes 20 min maximum based on field experience. Therefore, the boundary radial distances of 2–4 m are the most representative of field conditions. In this range, the difference between the numerical and theoretical shape factors is less than 10% (Fig. 12). The range of appropriate boundary radial distance may be different for the second series, but can be analyzed in the same way, and thus is not presented here.

The two series of VH tests were influenced similarly by the extended radial distance: They reduced from R = 2 to 8 m and kept constant at further distances. The second series has a filter pack, and it yields c values closer to the Hvorslev's c values compared to that of the first series.

At first sight, the shapes of the plots for VH and CH transient shape factors (Figs. 4, 7) seem similar. However, they represent different meanings: The decreased part from R = 2 to 8 m of the CH transient plot presents steady-state numerical c values, but the VH plot shows the sensitive c values affected by the varied R. When R exceeds 8 m, the flat part of the VH plot indicates a stable c value, whereas the CH transient plot becomes horizontal due to the insufficient test time.

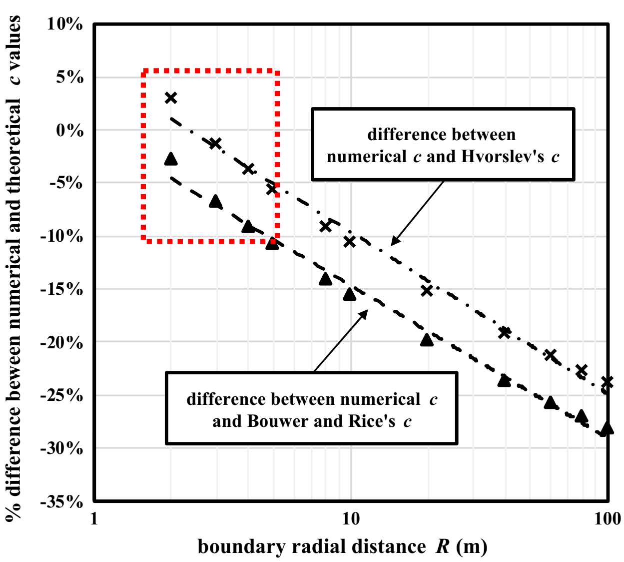

Fig. 12 Percentage differences between theoretical and numerical shape factors versus boundary radial distances (no filter pack)

Then, the problem arises, "What boundary radial distance should we define for the aquifer model to get correct shape factors or numerical results?" The answers are different for the two types of field permeability tests. For the CH test model, the first step is to build several trial models with different boundary radial distances, for example, 1, 3, and 5 m (based on the size of the model), and the second step is to find the one that has similar test duration as the field test. For the VH test model, the R at which the c value starts to become constant can be chosen as the appropriate R. For different geometries of aquifer models, the representative R may change.

5.2 Water injection zone dimension and position influence on shape factor

5.2.1 First series: no filter pack

The different lengths and positions of water injection zones were analyzed for the first-series models with boundary radial distances of 3 m. The theoretical and numerical c values are displayed in Fig. 13. The Hvorslev's shape factors are 1.79, 2.99, 4.09, and 5.14 m for injection zone lengths of 1, 2, 3, and 4 m, respectively. They do not depend on the position of the water injection zone. Bouwer and Rice's method yields the highest c values. They grow from 1.90 to 6.93 m corresponding to the increased length (from 1 to 4 m) and the rising positions (from lower to upper part of aquifer) of the injection zone. The VH test c values seem to follow the trend of the Bouwer and Rice's c, ranging from 1.97 to 6.13 m, which are 9 to 49% larger than the Hvorslev' c values. The CH steady-state and transient shape factors are identical and superpose in the

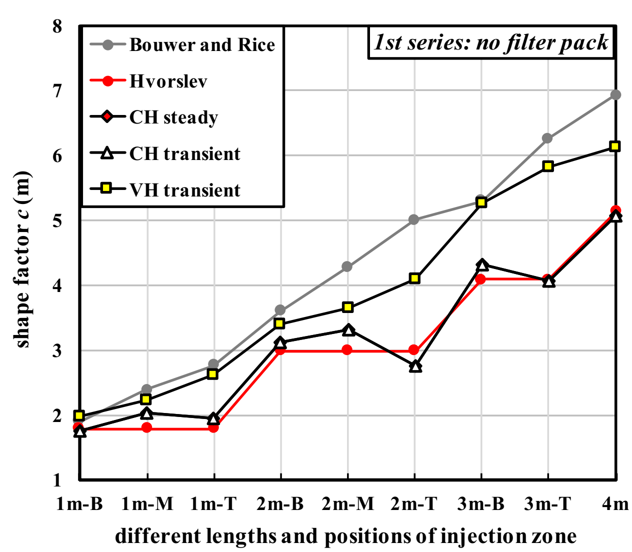

Fig. 13 Shape factors with regard to different injection zones (no filter pack)

plot. They are close to the Hvorslev's c values but somewhat differ from one another. The c of 1 m-M is 13% higher than the Hvorslev's c value, which is the greatest difference.

5.2.2 Second series: with a filter pack

The shape factor values for the second-series models are presented in Fig. 14. The Hvorslev's c values are 2.44, 3.85, 5.13, and 6.35 when the lengths of filter packs are, respectively, 1, 2, 3, and 4 m. The numerical c values of CH tests under two analyses are equivalent and deviate from the Hvorslev's c in the same way as the first-series models do. The largest deviation occurs in model 1 m-M, which is 12% higher. The Bouwer and Rice's c values are the highest in most cases except the 3 m-B, ranging from 2.55 to 8.87 m and present better consistency with the c values of VH test compared to the Hvorslev's c values. The VH test c values increased with the position of the water injection zone from 2.67 to 7.62 m, which are between 6 and 66% higher than the Hvorslev's c values.

5.2.3 Discussion

For each series of models, the shape factors increase when the lengths of the screen or filter pack increase. The second-series models yield higher c values than the first series due to the larger diameter of the water injection zone. The CH test c values for the two series are close to the Hvorslev's c values but have slight discrepancies, which is due to the equivalent boundary radial distance defined for altered water injection zones. For each water injection zone, the corresponding R should be customized. Under the conditions of R = 3 m, Bouwer and Rice's equations yield better consistency with the numerical VH test shape factors and therefore are higher than those of the CH tests. Based on the discussion in previous section, a numerically defined R value of 3 m is too small for the VH test models, especially for the water injection zones with 3- or 4-m lengths.

5.3 Material influence on numerical shape factors

5.3.1 First series: no filter pack

The initial No. 0 sand was replaced by Nos. 1 to 14 soils that are coarse, medium, fine, loamy sand, and silt. The numerical c values of models with the 14 aquifer materials are compared with the theoretical shape factors in Fig. 15. The numerical shape factors for CH tests are 1.77–1.78 m, 1% smaller than the Hvorslev's c value of 1.79 m when R is 3 m for the two series of models. They are also equivalent to that of the initial model with No. 0 sand (1.77 m), which indicates that the aquifer material has no effect on them. The VH test shape factors, ranging from 1.84 to 2.08 m, are more easily affected by the material properties. They are 3 to 16.4% higher than the Hvorslev's c when R = 3 m. When R increases to 10 m, the VH test c values stabilize and decrease by 2–4%.

5.3.2 Second series: with a filter pack

The filter material is the same for the 14 different aquifers. It has a much higher hydraulic conductivity than those of aquifers. Figure 16 presents the c values in the same order

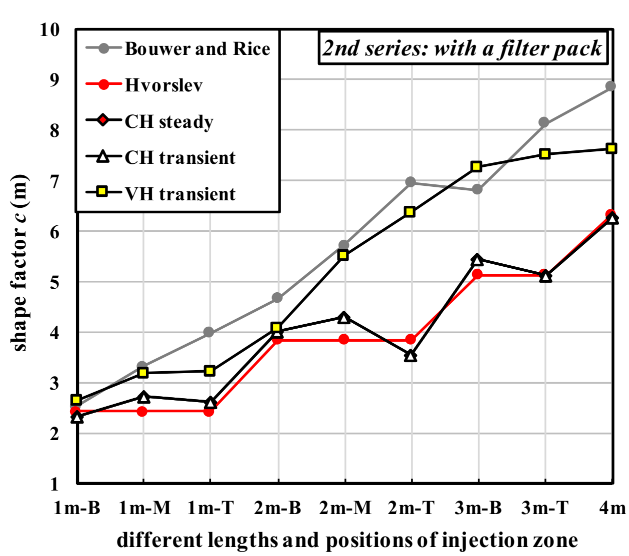

Fig. 14 Shape factors with regard to different injection zones (with a filter pack)

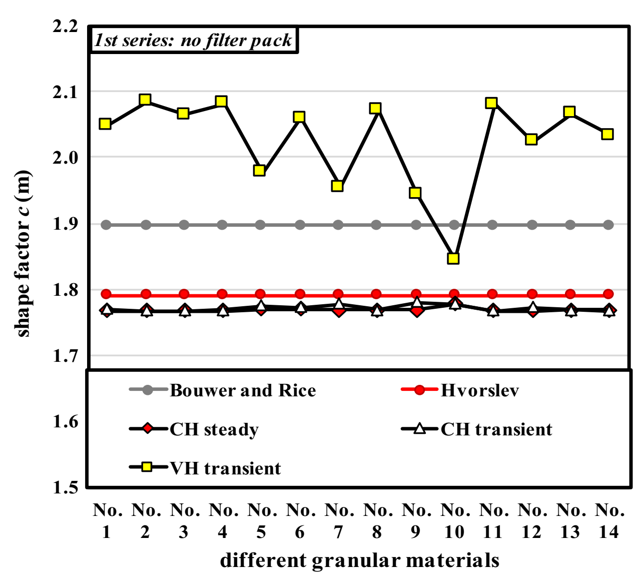

Fig. 15 Theoretical and numerical shape factors with regard to different materials (no filter pack)

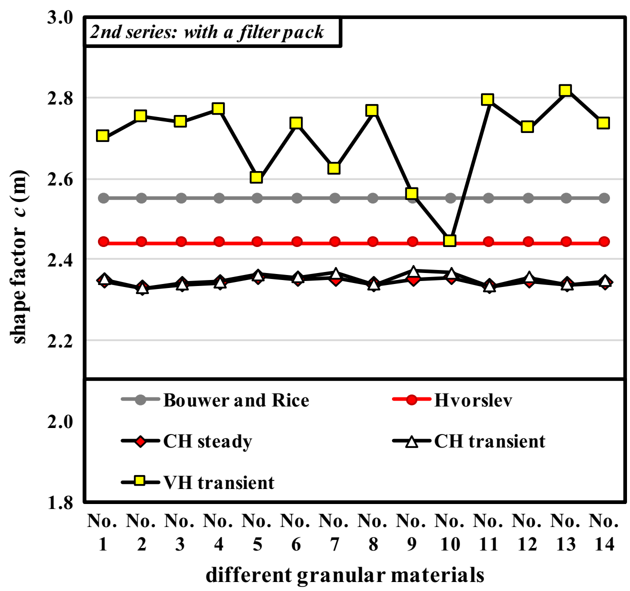

Fig. 16 Theoretical and numerical shape factors with regard to different materials (with a filter pack)

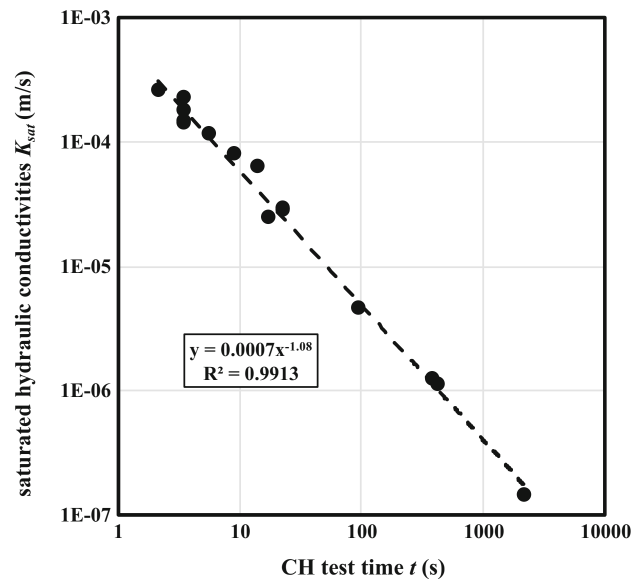

Fig. 17 Relationship between saturated hydraulic conductivities and CH test time (no filter pack)

as the first series. The CH tests of steady-state and transient analyses yield the lowest shape factors values between 2.33 and 2.37 m (nearly constant), 3–5% less than the Hvorslev's c when $R = 3$ m. Similar to the first series, the c values of the VH tests vary with the aquifer material. They are between 2.4 and 2.8 m, which increase by 0–15% compared to the Hvorslev's c when $R = 3$ m.

5.3.3 Discussion

The second-series models yield greater c values because of the filter pack. The two types of numerical analyses for the CH test gave very close shape factor values for each aquifer material, which implies that the test with a transient analysis reached stabilization for all models with R of 3 m. Although the CH transient analyses give nearly constant c values for different materials, the time to reach equilibrium for coarser sand is shorter than that for finer sand or silt due to its higher hydraulic conductivity. Figure 17 presents the duration of test time versus the aquifer material K_{sat} value. The test is considered as completed when the Q or H value reached 99% of the steady-state value. Thus, aquifer models with different materials need to be defined with different test times and boundary radial distances, which is also a trial-and-error process.

The two series of VH test c values have similar variation trend and show higher sensitivity to different aquifer material properties. The recovery phases of the VH tests were considered to be completed when the water in pipe returned to 3.002–3.004 m, which is around 0.1% different from the pretest water level (3 m). The recovery time for the first-series model was 27 s for No. 2 Berlin coarse sand, which has the highest K_{sat}, and reached 15 h for the No. 10 silt which is the least permeable. The second series of VH tests had similar relationship between the test time and the saturated hydraulic conductivity. The only difference is that the second-series VH test of each aquifer material used less time to recover than the corresponding first series due to its high permeable filter pack. The relationship between K_{sat} and VH test time follows a power function (Fig. 18), from which the VH test time can be deduced for any aquifer material with given K_{sat}.

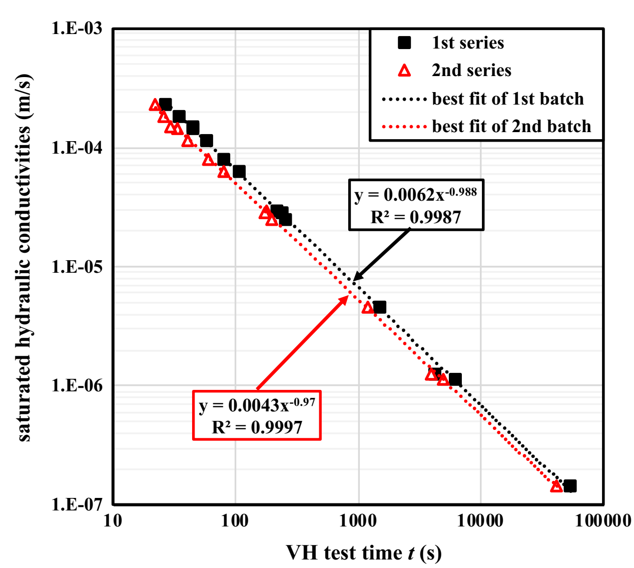

Fig. 18 Relationship between saturated hydraulic conductivities and VH test time (first series = no filter pack; second series = with a filter pack)

When we plot the VH test c values with their corresponding K_{sat} values (Fig. 19), a linear relationship between the c values and log K_{sat} was found. The two series of VH test shape factors increase nearly in parallel with the increase in the K_{sat} values. The small deviation is due to the slightly different post-test water level (3.002–3.004 m) used in test interpretation. The exact post-test water level is 3 m, which is the initial water level specified in the aquifer. The average difference in the two-series VH test c values in Fig. 19 is 0.67 m, which is close to the Hvorslev's c difference between the first and second series: 2.44 − 1.79 = 0.65 m.

6 Conclusion

The CH and VH tests in unconfined aquifers with impervious bottoms were numerically simulated using Seep/W, from which the numerical c values were calculated. The CH tests were modeled in steady-state and transient conditions. Each condition was simulated by applying the boundary condition of either a constant H or Q on screen, which yields a stabilized Q or H in the pipe, respectively, when reaching equilibrium. It corresponds to the two ways to conduct a field CH test. The numerical CH steady-state c value is not influenced by aquifer materials for the two-series models: with a screen only and with a screen surrounded by a filter pack. The c value increases when L and D of the water injection zone were increased, and varies slightly with the reduced distance to the unsaturated zone for fixed L and D. Among all the variables, the R value affects most on the numerical results (up to 35% for the second series when R = 100 m): The c values decline due to the reduced radial gradient. Specifying a large R value in a numerical model poorly represents the field conditions and largely increases the computation time.

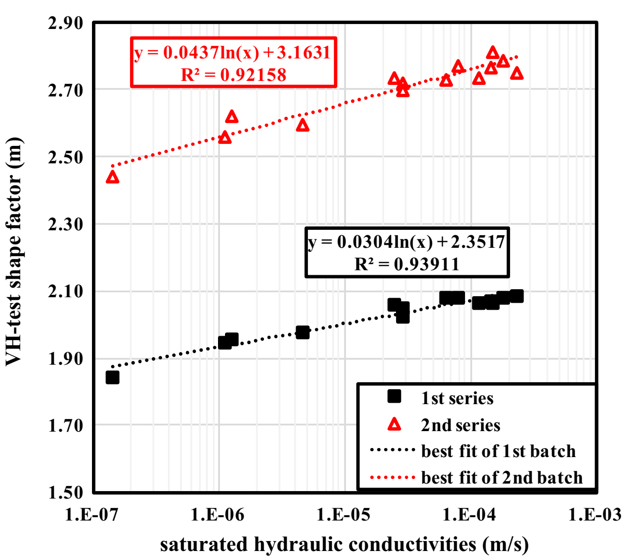

Fig. 19 Relationship between saturated hydraulic conductivities and VH test shape factor time (first series = no filter pack; second series = with a filter pack)

If CH tests reach equilibrium, the transient c values are influenced by the variables in the same way as the steady-state c values are. If not, they become invariable rather than decreasing for increased R. It indicates the first difference between the two CH test conditions: The transient analysis requires a much longer computation time. Therefore, if the CH test transient and steady-state models give different shape factors for each aquifer material, one needs to apply either a longer test time or a smaller boundary radial distance. The test time, however, should be in a realistic range.

The second difference is that the variation of H and Q values at any time during the transient model can be known. If your interest is the steady-state Q, to derive the numerical c value, a CH steady-state analysis is the right choice. It is simple and time-saving. If you target at studying the seepage at different times during the test, a CH transient analysis is needed.

Less permeable materials and larger R values need longer testing times, and vice versa. In this case, a long testing time may represent unrealistic field testing conditions, but an inadequate accuracy for a very small pumped flow rate also represents impractical field testing conditions. It is important to note that materials that have a $K_{sat} < 10^{-6}$ m/s are not suitable for a CH test [62], and those with test duration exceeding 1 h are uneconomic for field CH tests (Figs. 10, 11). These are practical recommendations for field CH tests.

The VH test c values are affected by R values differently, which decline first and stabilize at larger distances. The invariable numerical c values have differences smaller than 5% compared to Hvorslev's c values. Therefore, in practice, the test may be interpreted using the c value of Hvorslev [37] with confidence, even if the numerical c values present a linear small variation with log K_{sat} for the two series of VH tests.

The recovery time of the VH test and the CH test test duration are shorter for the high permeability aquifer material. The two parameters, K_{sat} and t, follow a power function relationship. The functions can be used to deduce the CH and VH test times for any material with a given K_{sat} for a certain series of models.

The R value of the aquifer model needs to be carefully specified because it may cause unrealistic results. Several practical recommendations to simulate CH tests are summarized: (1) build several trial models with different R values; (2) find the test time that reaches stabilization for each model by observing the Q or H variation in transient analysis; (3) compare the test duration with the one in practice to determine a proper range of R values. It also depends upon the aquifer material properties. A test time should be specified as a start and then adjusted to the proper one by trial and error. The R value of the VH test model is where the c value starts to be constant.

Additionally, the models with different aquifer materials were built with a single filter material. If the screen slot size is poorly selected or the filter material is poorly chosen, the shape factor is changed and the measured K_{sat} value is not that of the tested soil but a value lower than the maximum value that can be reached with this MW [4]. When a MW is poorly designed [63], the complex problem of the resulting shape factor is useless and was not investigated for this paper.

Acknowledgements The first author is grateful to the China Scholarship Council for its financial support. All authors would like to show their gratitude to the Natural Sciences and Engineering Research Council of Canada (NSERC) for sponsoring their research on field permeability tests and numerical studies.

References

1. Al-Dhahir ZA, Morgenstern NR (1969) Intake factors for cylindrical piezometer tips. Soil Sci 107(1):7–21
2. Ardejani FD, Badii K, Limaee NY, Mahmoodi NM, Arami M, Shafaei SZ, Mirhabibi AR (2007) Numerical modelling and laboratory studies on the removal of Direct Red 23 and Direct Red 80 dyes from textile effluents using orange peel, a low-cost adsorbent. Dyes Pigments 73(2):178–185
3. Aubertin M, Mbonimpa M, Bussière B, Chapuis RP (2003) A model to predict the water retention curve from basic geotechnical properties. Can Geotech J 40(6):1104–1122
4. Baptiste N, Chapuis RP (2015) What maximum permeability can be measured with a monitoring well? Eng Geology 184:111–118
5. Bouwer H (1989) Bouwer and Rice slug test—an update. Groundwater 27(3):304–309
6. Bouwer H, Rice RC (1976) A slug test for determining hydraulic conductivity of unconfined aquifers with completely or partially penetrating wells. Water Resour Res 12(3):423–428
7. Brand EW, Premchitt J (1980) Shape factors of cylindrical piezometers. Géotechnique 30(4):369–384
8. Brand EW, Premchitt J (1980) Shape factors of some noncylindrical piezometers. Géotechnique 30(4):536–537
9. Brand EW, Premchitt J (1982) Response characteristics of cylindrical piezometers. Géotechnique 32(3):203–216
10. Çelik B, Rowe RK, Ünlü K (2009) Effect of vadose zone on the steady-state leakage rates from landfill barrier systems. Waste Manag 29(1):103–109
11. Chapuis RP (1989) Shape factors for permeability tests in boreholes and piezometers. Ground Water 27(5):647–654
12. Chapuis RP (1998) Overdamped slug test in monitoring wells: review of interpretation methods with mathematical, physical, and numerical analysis of storativity influence. Can Geotech J 35(5):697–719
13. Chapuis RP (2004) Predicting the saturated hydraulic conductivity of sand and gravel using effective diameter and void ratio. Can Geotech J 41(5):787–795
14. Chapuis RP (2005) Numerical modeling of rising-head permeability tests in monitoring wells after lowering the water level down to the screen. Can Geotech J 42(3):705–715
15. Chapuis RP (2009) Numerical modeling of reservoirs or pipes in groundwater seepage. Comput Geotech 36(5):895–901
16. Chapuis RP (2009) Variable head permeability tests in monitoring wells: comparing the shape factor defined by Bouwer and Rice (1976) to the shape factor given by Hvorslev (1951). Geotech News 27(1):41–43
17. Chapuis RP (2012) Influence of element size in numerical studies of seepage: small-scale details. Geotech. News 30(1):32–35
18. Chapuis RP (2012) Influence of element size in numerical studies of seepage: unsaturated zones, transient conditions. Geotech. News 30(4):16–19
19. Chapuis RP (2016) Proof of multiplicity of solutions for groundwater seepage in recharged heterogeneous unconfined aquifers. Int J Numer Anal Methods Geomech 40(14):1988–2002
20. Chapuis RP (2017) Stress and strain fields for overdamped slug tests in aquifer materials, and resulting conservation equation. Int J Numer Anal Met 41(18):1908–1921
21. Chapuis RP (2017) A simple reason explains why it is so difficult to assess groundwater ages and contamination ages. Sci Total Environ 593:109–115
22. Chapuis RP, Aubertin M (2001) A simplified method to estimate saturated and unsaturated seepage through dikes under steady-state conditions. Can Geotech J 38(6):1321–1328
23. Chapuis RP, Bélanger C, Chenaf D (2006) Pumping test in a confined aquifer under tidal influence. Ground Water 44(2):300–305
24. Chapuis RP, Chenaf D (2002) Slug tests in a confined aquifer: experimental results in a large soil tank and numerical modeling. Can Geotech J 39(1):14–21
25. Chapuis RP, Chenaf D (2003) Effects of monitoring and pumping well pipe capacities during pumping tests in confined aquifers. Can Geotech J 40(6):1093–1103
26. Chapuis RP, Chenaf D, Acevedo N, Marcotte D, Chouteau M (2005) Unusual drawdown curves for a pumping test in an unconfined aquifer at Lachenaie, Quebec: field data and numerical modeling. Can Geotech J 42(4):1133–1144
27. Chapuis RP, Chenaf D, Bussière B, Aubertin M, Crespo R (2001) A user's approach to assess numerical codes for saturated and unsaturated seepage conditions. Can Geotech J 38(5):1113–1126
28. Chapuis RP, Dallaire V, Gagnon F, Marcotte D, Chouteau M (2007) Falling-head permeability tests in an unconfined sand aquifer. Geotech Test J 30(2):104–112
29. Chapuis RP, Masse I, Madinier B, Duhaime F (2015) Water-retention curves of coarse soils without organic matter: improved data for improved predictions. Geotech Test J 38(3):325–337
30. Chapuis RP, Paré JJ, Lavallée JG (1981) In situ variable head permeability tests. In: Proceedings of 10th international conference on soil mechanics and foundation engineering, pp 401–406
31. Chesnaux R, Chapuis RP, Molson JW (2006) A new method to characterize hydraulic short-circuits in defective borehole seals. Groundwater 44(5):676–681
32. Chiasson P (2005) Methods of interpretation of borehole falling-head tests performed in compacted clay liners. Can Geotech J 42(1):79–90
33. Chu-Agor ML, Wilson GV, Fox GA (2008) Numerical modeling of bank instability by seepage erosion undercutting of layered streambanks. J Hydrol Eng 13(12):1133–1145
34. Dachler R (1936) Grundwasserstromung. Julius Springer, Vienna
35. Geo-Slope Int Ltd (2012) SEEP/W for finite element seepage analysis: user's guide. Geo-Slope Int Ltd, Calgary
36. Haverkamp R, Zammit C, Bouraoui F (1997) Grizzly soil data bank, base de données de paramètres caractéristiques des sols. LTHE, Grenoble

37. Hvorslev MJ (1951) Time-lag and soil permeability in ground water observations. U.S. Army Eng Waterw Exp Stn, Vicksburg
38. Jin SW, Choo YW, Kim YM, Kim DS (2014) Seepage characteristics of a buttressed embankment with a low permeable foundation: centrifuge and numerical studies. Trans ASABE 57(2):463–477
39. Kallstennius T, Wallgren A (1956) Pore water pressure measurement in field investigations. In: Proceedings of the Royal Swedish Geotechnical Institute No. 13
40. Klammler H, Nemer B, Hatfield K (2014) Effect of injection screen slot geometry on hydraulic conductivity tests. J Hydrol 511:190–198
41. Kosugi KI (1994) Three-parameter lognormal distribution model for soil water retention. Water Resour Res 30(4):891–901
42. Kovács G (1981) Seepage hydraulics. Elsevier, Amsterdam
43. Lafhaj Z, Shahrour I (2002) Use of the electric analogy for the determination of the shape factor in complex soil conditions. Int J Phys Model Geotech 2(4):39–44
44. Lefranc E (1926) Procédé de mesure de la perméabilité des sols dans les nappes aquifères et application au calcul du débit des puits. Le Génie Civil 109(15):306–308
45. Lefranc E (1937) La théorie des poches absorbantes et son application à la détermination du coefficient de perméabilité en place et au calcul du débit des nappes d'eau. Le Génie Civil 111(20):409–413
46. Leij FJ, Alves WJ, van Genuchten MTh, Williams JR (1996) The UNSODA unsaturated soil hydraulic database. Version 1.0. US Environmental Protection Agency, National Risk Management Research Laboratory, Cincinnati. Report No.: EPA/600/R-96/095
47. Lowther G (1978) A note on Hvorslev's intake factors. Géotechnique 28(4):465–466
48. Mathias SA, Butler AP (2007) Shape factors for constant-head double-packer permeameters. Water Resour Res 43(6):1–7
49. Mbonimpa M, Aubertin M, Bussière B (2006) Predicting the unsaturated hydraulic conductivity of granular soils from basic geotechnical properties using the modified Kovacs (MK) model and statistical models. Can Geotech J 43(8):773–787
50. Mualem Y (1976) A catalogue of the hydraulic properties of unsaturated soils. Development of methods, tools and solutions for unsaturated flow with application to watershed hydrology and other fields. Technion Israel Institute of Technology, Haifa. Research Project 442
51. Randolph MF, Booker JR (1982) Analysis of seepage into a cylindrical permeameter. In: Proceedings of 4th international conference on numerical methods in geomechanics, pp 349–357
52. Ratnam S, Soga K, Whittle RW (2001) Revisiting Hvorslev's intake factors using the finite element method. Géotechnique 51(7):641–645
53. Raymond GP, Azzouz MM (1969) Permeability determination for predicting rates of consolidation. In: British Geotechnical Society conference on in-situ investigations in soils and rocks, pp 285–293
54. Selvadurai AP (2004) Fluid intake cavities in stratified porous media. J Porous Media 7(3):1–17
55. Silvestri V, Bravo-Jonard C, Abou-Samra G (2011) A note on Hvorslev's shape factor for a flush bottom piezometer in uniform soil. Geomech Eng 3(2):109–116
56. Silvestri V, Abou-Samra G, Bravo-Jonard C (2012) Shape factors of cylindrical piezometers in uniform soil. Groundwater 50(2):279–284
57. Silvestri V, Bravo-Jonard C, Abou-Samra G (2013) A note on the validity of Hvorslev's shape factors for well points and piezometers. Geotech Test J 36(1):138–145
58. Smiles DE, Youngs EG (1965) Hydraulic conductivity determinations by several field methods in a sand tank. Soil Sci 99(2):83–87
59. Tavenas F, Diene M, Leroueil S (1990) Analysis of the in situ constant-head permeability test in clays. Can Geotech J 27(3):305–314
60. Van Genuchten MT (1980) A closed-form equation for predicting the hydraulic conductivity of unsaturated soils. Soil Sci Soc Am J 44(5):892–898
61. Wilkinson WB (1968) Constant head in situ permeability tests in clay strata. Géotechnique 18(2):172–194
62. Zhang L, Chapuis RP, Marefat V (2019) Field permeability tests with inward and outward flow in confined aquifer. Geotech Test J. https://doi.org/10.1520/GTJ20170417
63. Zhang L, Chapuis RP (2019) Recovery test after a constant-head test in a monitoring well: interpretation methods and new findings. Eng Geol. https://doi.org/10.1016/j.enggeo.2019.105150